Chapter 2
Theory of Well Potential Traps in the IEC

2.1 Introduction

As described in Chap. 1, there are two basic types of IECs: ion injected or electron injected. The difference can be easily envisioned by examining Fig. 2.1. There the grid is held at a positive voltage relative to ground. Thus electrons are accelerated (injected) inward, making this an electron-injected type IEC. If the voltage on the grid is reversed, ions created in a plasma discharge between the grid and the walls are extracted and accelerated inward, creating an ion-injected type IEC.

It might seem that the two injection methods are similar. However, important differences occur due to the mass difference in the particles that are then effectively providing the inertia to electrostatically confine the other species. This difference will become more apparent in the analyses in this chapter. From a practical point of view, work by Farnsworth and Hirsch focused on ion-injected type IECs. The Bussard "Polywell" uses a magnetic field to confine electrons that create the potential trap which in turn accelerates ions inward. Thus, in effect, it too is an "ion-injected" type IEC. There are a number of variations of these two extremes, some of which will be discussed here. One word of caution – "injection" is a somewhat misleading terminology. If either electrons or ions are generated externally, a zero energy as they enter at the grounded chamber wall is desired to avoid their passing through the grid and simply hitting the opposite wall.

In this chapter, we concentrate on well potential formation in a spherical IEC. This discussion assumes that the ion source is such that a neutral background gas is not required, i.e., a fully ionized plasma is assumed. In contrast, as discussed in Chap. 1, almost all experiments to date have had a significant background neutral pressure, such that most fusion reactions occur between the ion beam and background neutrals. However, the plasma case analyzed here represents an ideal for future devices designed for higher power fusion operations where fusion reactions are ion beam–beam type. In that case, the reaction rate scales as the ion beam density squared. Because the input power mainly goes into ion beam formation, the beam density squared scaling allows higher fusion rates per unit power than linear

G.H. Miley and S.K. Murali, *Inertial Electrostatic Confinement (IEC) Fusion: Fundamentals and Applications*, DOI 10.1007/978-1-4614-9338-9_2,

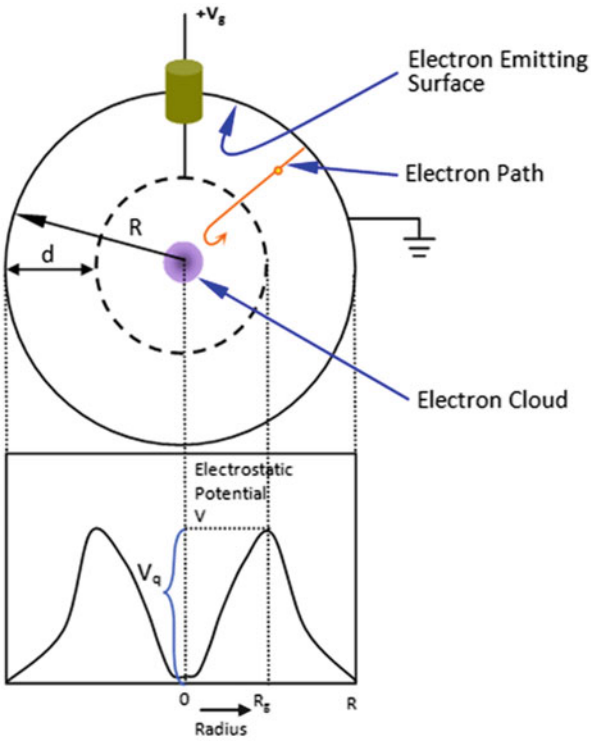

Fig. 2.1 Schematic representation of the "electron-injected" spherical device analyzed by Elmore et al. [1]

scaling. Also, charge exchange energy losses are essentially eliminated without background neutrals.

We begin by considering a conceptual illustration of the multiple well potentials first predicted by Farnsworth in Fig. 1.3 in Chap. 1. Figure 2.2a shows the potential diagram created by the cathode grid held at a negative potential relative to the vessel wall. This configuration automatically forms a well potential trap for ions. Because the objective is to accelerate an ion to its highest velocity as it passes through the center "core" of the device, the ion would ideally be born at the highest potential possible, i.e., very near to the wall. However, if ions are created by a plasma discharge between the grid and the wall, ions will be born over a range of potentials corresponding to the range of values between the wall and the cathode. This immediately brings up two key issues for IEC operation. First, if ions are "injected," a method must be developed to bring them into the grounded chamber at a potential slightly below ground or to cause them to lose energy in passing through the cathode grid (e.g., by collisions) such that they fall into this trap. Second, if a gas discharge is used, some method, such as electron source near the wall, is desirable to increase the ionization rate in that region. The point is that ions born near the wall (ground) gain a higher velocity versus the ones born elsewhere in the region between the grid and the wall. At the other extreme, an ion born near the cathode grid gains very little velocity. Here we will assume as shown in Fig. 2.2a that the

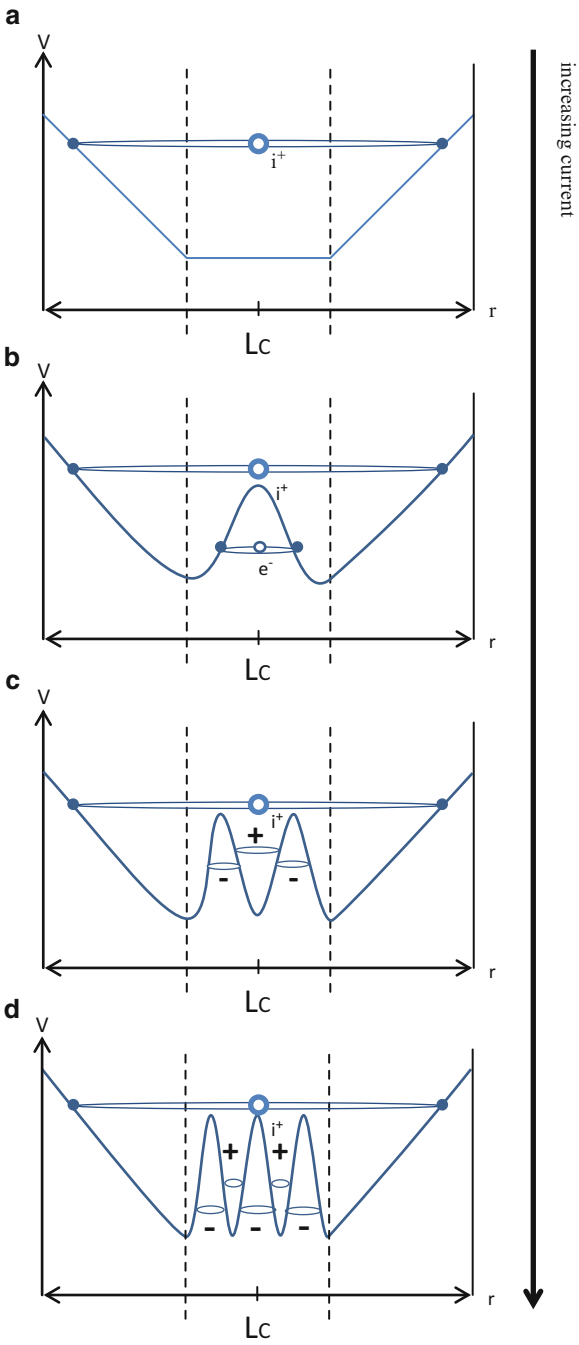

Fig. 2.2 Illustration of the formation of multiple well potentials in a spherical IEC as a function of increasing current in going from (**a**) to (**d**)

ions are produced at a potential surface near the wall. If the ion source rate is low, i.e., the ion current is low, the associated space charge created will not affect the potential, and the ion will circulate in the trap until it collides with the grid or suffers a collision with another ion such that its energy is increased, causing it to upscatter out of the potential trap (see Fig. 2.2a). However if the ion current is increased, the ion density will significantly increase near the center region of the spherical device due to a three-dimensional compression (or focusing) of the ion current in the center region. This will cause the corresponding formation of a virtual anode due to the high positive charge density in that region (see Fig. 2.2b). As the ion source rate continues to increase, the space charge can approach the value of the potential surface of the circulating ions, whereupon it will cause ions to be reflected before reaching the center virtual anode. However, the virtual anode serves as a well potential trap for electrons that are drawn into that region and circulate within this trap, much as the ions do in the outer trap. They in turn have a high density at the center line due to tight focusing in the spherical geometry. This results in the formation of a virtual cathode at the center line as shown in Fig. 2.2c. Ions are trapped in the well potential. Then, as illustrated in Fig. 2.2d, a new virtual anode is formed. In principle, this process could continue giving the nested "onion skin"-like virtual electrodes shown earlier in Fig. 1.3. As already noted, Farnsworth termed these nested well potentials "Poissors." However, in practice, as pointed out earlier, due to the ion energy spread in angular momentum effects, the potential trap formed by electrons (such as shown in Fig. 2.2c) is all that might be expected. Such a configuration leads to a maximum fusion reaction rate within each of the three ion traps, and that has been confirmed in measurements by Gu et al. [2] as described next.

Gu studied the fusion rate profiles to infer the potential trap profile [2]. This is based on the way the well potential profile affects the fusion reaction rate profile, as shown conceptually in Fig. 2.3.

In their experimental study, Gu and Miley [2] used a microchannel proton collimator to map out the fusion reaction rate profile as a function of ion current. The protons recorded were the 3.0-MeV protons created in D–D reactions. Gu et al. first studied the well potential and fusion reaction rate relationship using a computer simulation code (IXL) that solves the collisionless Vlasov equation and Poisson's equation in spherical coordinates [3]. That study confirmed that "practical" spreads in ion energy and angular momentum limit the number of spatially alternating wells to two (termed here a "double well" and illustrated in Fig. 2.3c). This double well is composed of a positive well by ions converging at the focal spot in the spherical cathode, with a negative well formed by electrons focused inside the positive well due to the virtual anode. While this double well falls short of the multiple well "Poissor" structure originally envisioned by Farnsworth, as a practical matter, it is capable of efficiently trapping ions within the virtual anode, much as hoped for in multiple wells. Thus the double well provides an attractive goal for future IEC devices designed for increased fusion rates. Due to this ion-trapping effect, the radial distribution of the fusion reaction rate density provides a means of distinguishing the double well profile.

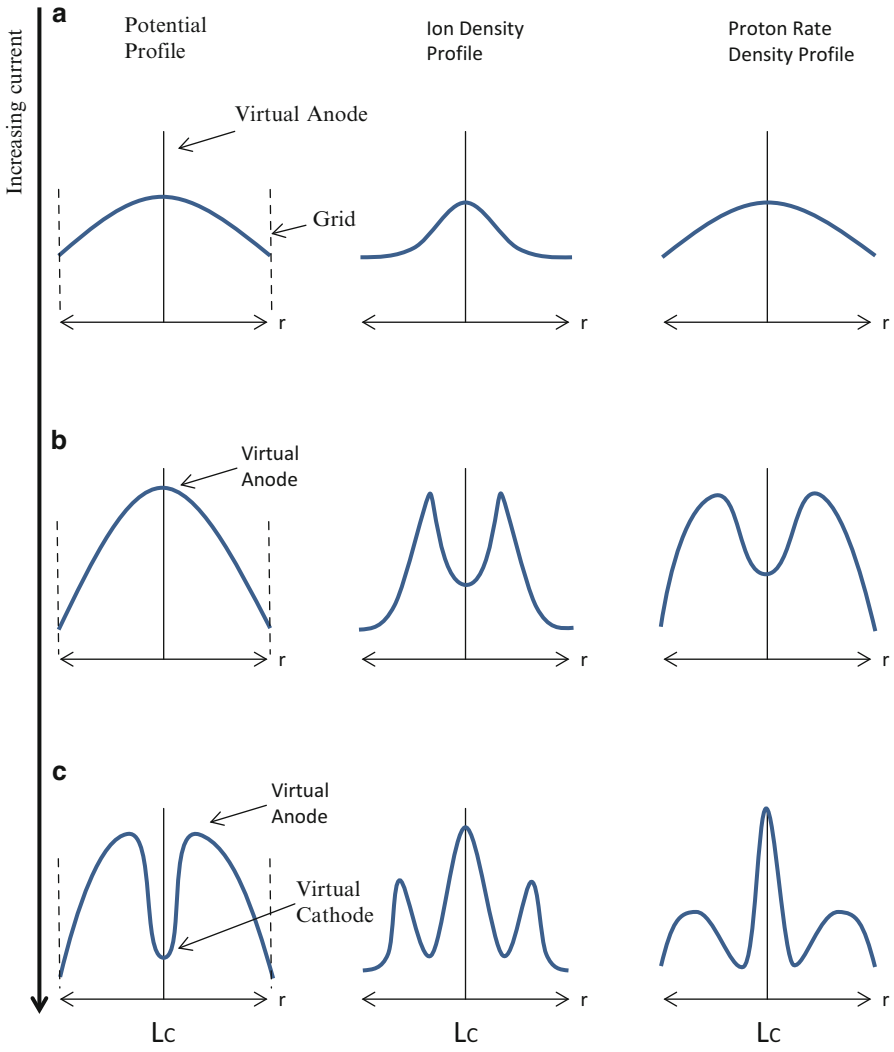

Fig. 2.3 An illustration of the changes in (**a**) proton rate density, (**b**) ion density, and (**c**) potential profile as the ion current increases [2]

The relation between the proton source-rate density profile and the well potential structure is delineated in Fig. 2.3 as a function of ion current. A fixed voltage is assumed in these figures. Note that the well potential properties follow the same pattern as shown earlier in Fig. 2.2, but now the corresponding fusion rate profiles are added to the right of the potential plots. The progression toward a double well is associated with increasing the ion current going from 2.3a to c. At low-ion current (such as in Fig. 2.3a), where the space charge potential at the center is low, a single sharp peak in the reaction rate density occurs there. As the height of this positive

potential peak increases in Fig. 2.3, ions are repulsed, causing a distinct "dip" in the reaction rate density peak at the center. However, as the ion current is further increased in Fig. 2.3c, the resulting virtual anode accelerates and focuses electrons in the center of the positive well, creating a potential "double well" (corresponding to the earlier Fig. 2.2c). Consequently, a distinctive peak in the reaction rate density suddenly appears in the middle of the dip in the reaction rate density profile due to the fusion of ions trapped by the double well. While the amplitudes of the various profiles will vary, the trends depicted will occur regardless of whether beam–beam or beam–background neutral-type fusion reactions dominate. Thus, these characteristics are quite general.

Because of the distinct reaction rate density behavior illustrated by Fig. 2.3, the experimental observance of two proton source-rate peaks (Fig. 2.3c) uniquely signals the existence of a double well potential. In addition, as discussed by Gu et al. [2], analysis of the reaction rate peak amplitudes can provide a reasonable estimate of the well depth.

Now that we have obtained a conceptual picture of well potential formation processes and the corresponding effect on the fusion reaction rate, we move on to review theoretical studies of this well potential formation in more detail.

An early theoretical analysis of IECs was carried out by Elmore, Tuck, and Watson [1]. At this point we present and extend their analysis because it leads to analytical solutions that illustrate the electrostatic structure of an IEC. The various assumptions employed in this analysis (and in other analytical solutions) limit the accuracy of the result. Thus, numerical methods such as discussed in Chap. 13 have been used for more realistic solutions. In their analysis, Elmore, Tuck, and Watson assumed electrons were injected radially inward with an energy of eV_o at the surface of a sphere. The electrons were then assumed to be stopped by their mutual repulsion near the center of the IEC and be reflected back toward the outer surface (analogous to the case for ion injection shown earlier in Fig. 2.2). The corresponding electrostatic potential within the sphere was shown earlier in Fig. 2.1. Elmore, Tuck, and Watson argued that a well potential of depth V_o will exist at the center, so positive ions of energy $\varepsilon_i < eV_o$ are confined within the well.

For reasonable confinement a well depth of $V_o \cong 100$ keV was assumed. This corresponds to an ion energy near the peak of the fusion cross section for D–T fusion reactions. Elmore and colleagues assumed all particles have radial motion (no angular momentum), neglected scattering collisions, and background neutrals (i.e., represents a fully ionized plasma), and potential surfaces were taken to be spherically symmetric (i.e., perturbations due to the "stalk" fixed to the grid to both hold it mechanically and supply a voltage to it). In a high vacuum where the electron mean free path is large compared to the grid diameter, an electron can make a number of passes before it collides with the grid and is lost. Owing to these recirculations, the effective space charge current given by the input current is multiplied by the average number of recirculations an electron makes. In other words, if an electron makes γ oscillations (across the grid), then the internal electron current drawn to the grid would be γ times the current drawn to the grid.

The suitable equation for describing the electrostatic equilibrium of such a potential distribution is the Poisson's equation. The electrostatic equilibrium of such a system is computed for two situations where the plasma has (1) a zero temperature and (2) a finite temperature. We now proceed to solve it for the zero plasma temperature assumption.

The Poisson's equation that describes the system in static operation is

$$\frac{1}{r^2}\frac{\partial}{\partial r}\left(r^2\frac{\partial V}{\partial r}\right) = -4\pi[\rho_i - \rho_e]. \tag{2.1}$$

Here i represents an ion and e represents an electron, ρ_i, ρ_e are the respective charge densities, and $\pm\nu_e$, $\pm\nu_i$ are the radial velocities at a given radius r. The total electron current (I_e) directed outward (and hence inward as well) is given by

$$I_e \equiv 4\pi r^2\left(\frac{\rho_e}{2}\right)\nu_e, \quad \text{and, similarly,} \quad I_i \equiv 4\pi r^2\left(\frac{\rho_i}{2}\right)\nu_i. \tag{2.2}$$

where the subscript e represents electrons and i represents ions. Conservation of energy requires that

$$\frac{1}{2}m_e{\nu_e}^2 - eV = \varepsilon_{oe}, \quad \text{and}$$

$$\frac{1}{2}m_i{\nu_i}^2 + eV = \varepsilon_{oi}. \tag{2.3}$$

Here m_e is the electron mass, m_i is the ion mass, e is the electron charge, and V is the electrostatic potential; ε_{oe} and ε_{oi} are the total energies, respectively, of an electron and ion.

A convenient dimensionless variable, W_e, associated with the electron energy, was proposed by P. T. Farnsworth [4] to simplify the analysis. He defined

$$W_e = \frac{\frac{1}{2}m_e{v_e}^2}{\Lambda}. \tag{2.4}$$

Here Λ is a constant parameter that has the dimensions of energy which will be determined later in the derivation. Solving for the radial velocities gives

$$v_e = \left(\frac{2\Lambda}{m_e}\right)^{\frac{1}{2}}W^{\frac{1}{2}} \text{ and } v_i = \left(\frac{2\Lambda}{m_i}\right)^{\frac{1}{2}}[W_o - W]^{\frac{1}{2}}, \tag{2.5a}$$

where

$$W_o \equiv \frac{1}{\Lambda}[\varepsilon_{0e} + \varepsilon_{0i}]. \tag{2.5b}$$

Equation 2.2 may be solved for ρ_e and ρ_i in terms of ν_e and ν_i, which in turn may be eliminated with Eq. 2.5a. We then obtain

$$4\pi e[\rho_i - \rho_e] = -\frac{2eI_e}{\left(\frac{2\Lambda}{m_e}\right)^{\frac{1}{2}}}\frac{1}{r^2}\left[\frac{1}{W^{\frac{1}{2}}} - \frac{G_0}{[W_0 - W]^{\frac{1}{2}}}\right], \tag{2.6a}$$

where G_0 is a function of the ion to electron current ratio:

$$G_0 \equiv \frac{I_i}{I_e}\left(\frac{m_i}{m_e}\right)^{\frac{1}{2}}. \tag{2.6b}$$

Returning to the Poisson's Equation 2.1 and setting $e\left(\frac{\partial V}{\partial r}\right) = \Lambda\left(\frac{\partial W}{\partial r}\right)$, we then obtain

$$\frac{\partial}{\partial r}\left(r^2\frac{\partial W}{\partial r}\right) = \frac{1}{W^{\frac{1}{2}}} - \frac{G_0}{[W_0 - W]^{\frac{1}{2}}}, \tag{2.7}$$

if we define the parameter Λ as

$$\Lambda^{\frac{1}{2}} = \sqrt{2}eI_e(m_e)^{\frac{1}{2}}. \tag{2.8}$$

For convenience, this equation can be expressed in terms of the independent variable

$$z \equiv \ln\frac{r}{r_o}. \tag{2.9}$$

Here r_o is a parameter which is characteristic of the "width" of the central region of the well potential. Equation 2.7 then becomes

$$\frac{d^2W}{dz^2} + \frac{dW}{dz} = \frac{1}{W^{\frac{1}{2}}} - \frac{G_0}{[W_0 - W]^{\frac{1}{2}}}, \tag{2.10}$$

with the boundary condition

$$\frac{\partial W}{\partial z} = 0 \quad \text{for } z = 0. \tag{2.11}$$

This equation represents a convenient form for the original Poisson's equation given in Eq. 2.1. A solution to Eq. 2.10 is most easily obtained for the simplest case, where $G_o = 0$, i.e., where the ion current is zero. For example, Elmore, Tuck, and Watson found for this case that with a well potential of depth $V_o \cong 100$ keV and

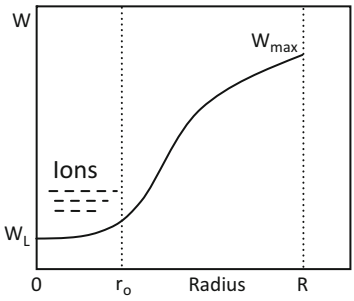

Fig. 2.4 The confinement of ions near the center "core" of the IEC well potential [4]

radius $r_o \cong 1$ cm can be maintained in a sphere 1 m in diameter with an electron current $(1/\nu)\, I_e \cong 100$ A.

However, this result poses some serious problems. The center of the well potential is restricted to a very small volume compared with the total volume within the sphere. Thus the volume of the confined fusion plasma is quite small, limiting the total fusion power level. This restriction occurred, however, by assuming that the electrons have no angular momentum about the center of the sphere. In fact, the electrons will develop transverse motion from scattering (deflection) by the accelerating grid and from scattering against the ions. While that will increase the central core fusing volume, the electron current must be increased to fill the volume at the high currents involved, and questions about instabilities must be studied. Indeed, one reason the Bussard "Polywell" IEC employs magnetic confinement of the electrons is to stabilize the electron well potential over a larger central volume.

Next, we consider Eq. 2.10 for the case when $G_o \geq 0$. If we integrate Eq. 2.10 outward from $z = 0$, W will increase from its value W_L at $z = 0$. As $W \rightarrow W_o$, the second term will dominate on the right-hand side of Eq. 2.10, causing W to start decreasing again. Thus, W never reaches the value W_o. This means that the well potential depth never becomes large enough to confine ions at W_o (see Eq. 2.5). Physically, this means that the ion charge density always dominates the electron charge density. This difficulty arises because the ions have all been given a single energy ε_{oi} as specified by Eq. 2.3. On the other hand, if the ions are injected with a distribution of energies ε_{oe} or if they are injected sufficiently slowly for a wider distribution to develop due to scattering, this issue may be resolved. Indeed, Elmore and colleagues state that it may be possible to have a system for which W is not bounded from above by the ion charge density. This issue of satisfying boundary conditions is common in such problems; e.g., it is encountered again in Hirsch's analysis of an ion-injected system [5]. The region found by his analysis where the boundary condition is satisfied and is presented graphically in Fig. 2.4.

2.2 Ion Velocity Distribution

Elmore and colleagues also studied the effect of electron angular momentum on ion velocity distribution in the system. Following various approximations, they concluded that the cumulative effect of small-angle scattering of electrons on electrons and ions will give a small displacement from the core size for zero angular momentum. However, they found that it was probably not large enough to be serious. On the other hand, they found ion collisions may cause the ions to relax into a roughly Maxwellian form that can be represented as a radial Maxwell distribution. This is employed to evaluate the fusion reactivity $\langle \sigma \upsilon \rangle$ in the following fusion power calculations. Under these conditions the intrinsic difficulty of obtaining sufficient ion density remains. (For details of this derivation, see reference [1].)

If the ions are distributed according to a Maxwell distribution with temperature θ, then the ion density as a function of r will be

$$n_i \approx n^o \exp\left(-\frac{eV}{\theta}\right) \cong \left[n_o{}' \exp\left(\frac{W_L}{\rho}\right)\right] \exp\left(-\frac{W}{\rho}\right), \tag{2.12}$$

with

$$\rho = \frac{\theta}{\Lambda}, \tag{2.13}$$

and W_L is the value of W at $r = r_o$. Here n_o and $n_o{}'$ are constants, $n_o{}'$ being the density at $r = r_o$. On the other hand, for only radial velocities and for the distribution of ε_{oi} values $P(\varepsilon_{oi})\, d\varepsilon_{oi}$, the distribution function in r and υ_i space is

$$f(r, \upsilon_i) = \frac{C}{r^2} P\left(\frac{1}{2} m_i {\upsilon_i}^2 + eV\right), \tag{2.14}$$

with

$$n_i(r) = \int f(r, \upsilon_i) d\upsilon_i. \tag{2.15}$$

For our subsequent discussions, we shall take

$$n(r) = n_o {r_o}^2 \frac{\exp\left(-\frac{W}{\rho}\right)}{r^2}. \tag{2.16}$$

Equation 2.16 corresponds to a radial Maxwell distribution and is viewed as a "conservative approach" relative to the optimum performance of the electrostatic system.

The distribution function of Eq. 2.16 will be used rather than Eq. 2.12 for the present calculations. The reason for this is mathematical. With Eq. 2.16 we can obtain the parameters of an "optimum system" in closed form. Because the ratio $(r_o/r)^2$ is limited in its variation in a practical device, we do not expect any appreciable difference in the operation of the two systems given by Eqs. 2.12 and 2.16. Finally, Eq. 2.16 is in any case optimistic for the behavior of the device. That is, the intrinsic difficulty is to obtain a sufficient ion density for thermonuclear reactions at the center and, at the same time, a low enough ion density elsewhere that the charge density remains negative. With the new distribution function of Eq. 2.16, we may rederive the appropriate Poisson's equation. In place of Eq. 2.11, we now obtain

$$\frac{d^2W}{dz^2} + \frac{dW}{dz} = \frac{1}{W^{\frac{1}{2}}} - G\ \exp\left(-\frac{W}{\rho}\right), \tag{2.17}$$

where

$$G \equiv \frac{2\pi n_o e r_o^2}{I_e}\left(\frac{2\Lambda}{m_e}\right)^{\frac{1}{2}}. \tag{2.18}$$

Here Λ is defined by Eq. 2.8.

Next we discuss how this system of equations restricts the fusion power density. Then we turn to subsequent studies by Farnsworth and Hirsch and review how they treat this ion density limit to obtain a more promising result.

2.3 Conditions for Maximum Thermonuclear Power

In this section we summarize Elmore and colleagues' evaluation of the maximum fusion power allowed in their model of the electron-injected potential trap.

The power input P_i to the device is the grid current times the grid voltage, divided by γ, the number of times an average electron goes into the control region of the device, or

$$P_i = \frac{1}{\gamma} I_e V_g, \tag{2.19}$$

where I_e and V_g are expressed in esu.

The thermonuclear power output P_o is

$$P_o = \left[\frac{4\pi}{3} r_o^3\right] \times \left[\frac{n_o^2}{4} < \sigma_{DT} v >_{avg} \Delta\varepsilon\right]. \tag{2.20}$$

Here $\frac{4\pi}{3}r_o^3$ is the active volume in which reactions occur; $< \sigma_{DT}\upsilon >_{avg}$ is the product of relative velocity and the D–T reaction cross section averaged over a Maxwellian velocity distribution for the ions (here we assume D–T reactions instead of D–D reactions as they have a larger cross section, giving a higher fusion power); and $\Delta\varepsilon$ is the energy liberated in a D–T reaction and is taken as

$$\Delta\varepsilon = 15 \text{ MeV}, \tag{2.21}$$

and

$$\frac{n_o^2}{4} = n_D n_T. \tag{2.22}$$

Here n_D and n_T are the respective densities of deuterons and tritons.

Equation 2.20 is subject to a geometric correction factor of order unity, because $\frac{4\pi}{3}r_o{}^3$ gives only an approximate value for the reaction volume. Then the ratio of fusion power out to the input power, P_o/P_i, must exceed unity for breakeven. This ratio is given by

$$\frac{P_o}{P_i} = \frac{n_o^2 r_o^3 \left[\frac{\pi}{3}\Delta\varepsilon < \sigma\upsilon >_{avg}\right]}{I_e V_g} v > 1. \tag{2.23}$$

The largest ion density for which ion containment is possible corresponds to the largest value of G in Eq. 2.17 for which W is not bounded from above. This case was illustrated earlier in Fig. 2.4, where the ions are shown as confined to the bottom of the potential well.

To analyze this further, Eq. 2.17 is multiplied by $p = \frac{dW}{dz}$ giving us

$$\frac{dW}{dz}\left(\frac{d^2W}{dz^2} + \frac{dW}{dz}\right) = \frac{d}{dz}\left(\frac{p^2}{2}\right) + p^2 = \frac{dW}{dz}\left(\frac{1}{W^{\frac{1}{2}}} - G\exp\left(-\frac{W}{\rho}\right)\right). \tag{2.24}$$

With $W = W_L$ and $p = 0$ at $z = 0$, we integrate out from $z = 0$ to obtain

$$\begin{aligned}\frac{p^2}{2} + \int_0^z p^2 dz &= \int_{W_L}^{W}\left[\frac{1}{W^{\frac{1}{2}}} - G\ \exp\left(-\frac{W}{\rho}\right)\right]dW \\ &= \left\{2\left[W^{\frac{1}{2}} - (W_L)^{\frac{1}{2}}\right] - \rho G\left[\exp\left(-\frac{W_L}{\rho}\right) - \exp\left(-\frac{W}{\rho}\right)\right]\right\}.\end{aligned} \tag{2.25}$$

Because $\int p^2 dz > 0$, we have

$$\frac{p^2}{2} \geq \left\{ 2\left[W^{\frac{1}{2}} - (W_L)^{\frac{1}{2}} \right] - \rho G \left[\exp\left(-\frac{W_L}{\rho} \right) - \exp\left(-\frac{W}{\rho} \right) \right] \right\} \equiv F(W). \quad (2.26)$$

Clearly, *F(W)* must be positive for all $W_L < W < W_{\max}$. This implies an upper limit on G. Because of the range of parameters involved (for confinement $W_{\max} >> \rho$), it will suffice to take

$$\begin{aligned} W_L &= 0, \\ W_{\max} &= \infty. \end{aligned} \quad (2.27)$$

Hence we now have from Eq. 2.26

$$F(W) = 2\left\{ 2W^{\frac{1}{2}} - \rho G \left[1 - \exp\left(-\frac{W}{\rho} \right) \right] \right\}. \quad (2.28)$$

Now the least value of F is given by

$$\frac{dF}{dW} = 0. \quad (2.29)$$

Defining a root $W = W_R$, the condition Eq. 2.26 implies that

$$F(W_R) \geq 0. \quad (2.30)$$

If we write

$$Q = \rho^{\frac{1}{2}} G, \quad (2.31)$$

then Eq. 2.29 becomes

$$1 = Qx \times \exp\left(-x^2\right). \quad (2.32)$$

Here $x^2 \equiv (1/\rho) W_R$. Then the equation $F(W_R) = 0$ gives

$$Q = \frac{2x}{1 - \exp(-x^2)} \quad (2.33)$$

The solution of Eqs. 2.32 and 2.33 is

$$Q = \rho^{\frac{1}{2}} G_{\max} \approx \pi$$

or

$$G \leq \left(\frac{\Lambda}{\theta} \right)^{\frac{1}{2}} \pi. \quad (2.34)$$

If we now substitute Eq. 2.18 in Eq. 2.34, we find

$$n_o \leq \left(\frac{m_e}{\theta}\right)^{\frac{1}{2}} \frac{I_e}{2^{\frac{3}{2}} e {r_o}^2}. \tag{2.35}$$

This result provides the upper limit on the ion density n_o in the central "core" region of the spherical system.

The power ratio from Eq. 2.23 will be greatest if we use the largest possible ion density, given by making Eq. 2.35 an equality. Substituting into Eq. 2.23 for n_o, we obtain

$$\frac{m_e}{\theta} \frac{{I_e}^2}{e^2 r_0} \frac{\left[\frac{\pi}{24} \Delta\varepsilon \langle\sigma v\rangle_{avg}\right]}{I_e V_g} > \frac{1}{\gamma}. \tag{2.36}$$

Next, we set

$$eV_g \cong 5\theta, \tag{2.37}$$

where θ is the average ion temperature. The value of eV_g cannot be much less than this, or the ions will not be confined. In addition, a larger value cannot be used because of the inequality Eq. 2.36. Now, substituting Eq. 2.37 into Eq. 2.36, we obtain

$$\frac{\pi}{120} \frac{m_e I_e \Delta\varepsilon}{e r_0} \frac{\langle\sigma v\rangle_{avg}}{\theta^2} > \frac{1}{\gamma}. \tag{2.38}$$

The next step is to find the temperature where $\theta = \theta_o$, which maximizes the ratio

$$\frac{\langle\sigma v\rangle_{avg}}{\theta^2}.$$

As shown in reference [4], this occurs for D–T reactions when

$$\begin{aligned} &\theta \cong 40 \text{ keV}, \\ &\langle\sigma v\rangle_{avg} \cong 7.2 \times 10^{-16} \text{cm}^3/\text{s}. \end{aligned} \tag{2.39}$$

Substituting these values into the inequality 2.38, we find

$$I_e > 10^{25} \frac{r_o}{\gamma} \text{esu}, \tag{2.40}$$

or

$$I_{amp} > 10^{16} \frac{r_o}{\gamma} \text{ A}.$$

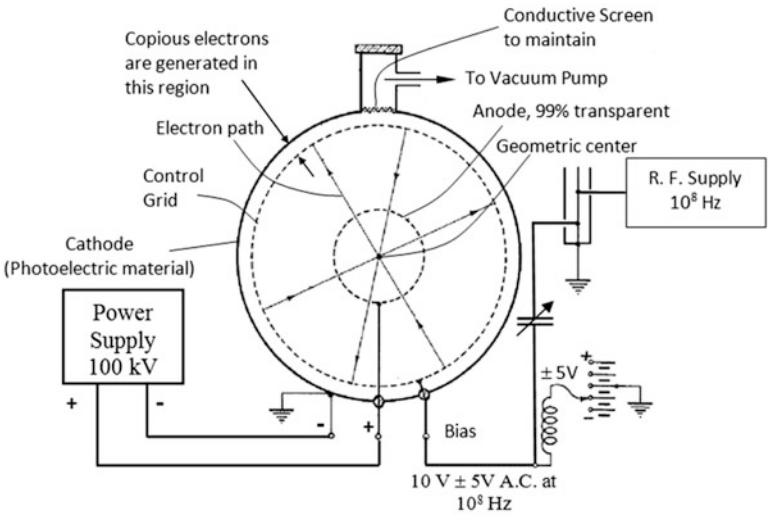

Fig. 2.5 IEC geometry proposed by P. T. Farnsworth [6]

From earlier discussion, it may be found that $\frac{r_o}{\gamma}$ is roughly 10^{-2}. Hence, from this analysis, it may be concluded that currents of the order of 10^{14} A are required for successful operation of the IEC described. This is an enormous current and practically impossible to realize, at least in the geometry considered. Even pulsed operation of the device might not be able to reach this current. Therefore, a system employing electrons injected into a transparent grid to confine ions seems to be impractical for useful fusion power. However, Elmore and colleagues conclude with the statement that other configurations and assumptions are still open for analysis. And that is what Philo Farnsworth attempted to do in his pioneering study of IEC fusion discussed next.

2.3.1 The Farnsworth "Fusor"

Farnsworth proposed a space charge device for producing nuclear reactions (shown in Fig. 2.5). He first proposed that the electric fields within the space charge would oscillate the ions resulting in collisions of particles and thus producing nuclear fusion. His design used concentrically arranged cathode and anode elements, the anode being electron permeable and supported within the cathode element. Farnsworth's design is very similar to the one analyzed by Elmore, Tuck, and Watson but with some subtle differences. One is that Farnsworth proposed a space charge buildup at the center causing a virtual cathode. Furthermore, he stated that ions are formed in the anodic space (inside the anode) through electron collisions

with background neutrals. Such ions fall through the negative virtual well potential resulting in their acceleration to high fusion–relevant energies.

Farnsworth argued that a virtual cathode potential, almost the same potential as that of the cathode, can be established within the anode through space charge buildup. This, he concluded, would be possible with the application of a 100-kV and 1,500-A electron current. In this case, the instantaneous space current, including both inward and outward flow, is related to the cathode current by the following series:

$$I_{space} = I_{cathode} \sum_{0}^{\gamma} \eta^{\gamma}, \tag{2.41}$$

where

$$\eta \equiv \frac{A_O}{A_{anode}}. \tag{2.42}$$

Here A_O is the open anode area, A_{anode} is the total anode area, and γ is the number of trips through the anode in both directions made by an electron that started at the cathode.

The variation in space current with time may be found by determining the electron transit time t for an electron between its inner and outer limits of travel, because this determines how often it passes the anode. Then the current at a specified time T is determined by substituting

$$\gamma = \frac{T}{t}. \tag{2.43}$$

The relation between the anode current and cathode current is then given as

$$I_{anode} = I_{cathode}(1 - \eta) \sum_{0}^{\gamma} \eta^{\gamma}. \tag{2.44}$$

From Eqs. 2.42 and 2.44, we obtain

$$I_{anode} = I_{space} \times (1 - \eta). \tag{2.45}$$

Hence, the actual space current in the device is many times greater than the anode current by a factor corresponding to $1/(1-\eta)$. Therefore, for $\eta = 99$ %, this factor is 100 giving anode current of only 15 A needed to supply the 1,500-A space current requirement. Assuming a spherical symmetry in the creation of the space charge, Farnsworth claimed that it is possible with this space charge flow to produce the desired nonuniform potential distribution in a space enclosed by a permeable equipotential surface (anode).

In order to obtain a copious electron current from the cathode, Farnsworth suggested that the cathode be built with either aluminum or with copper, having its interior coated with aluminum. Such a material would emit copious amounts of

electrons when bombarded with UV radiation. As the gas atoms (in a previously evacuated cathode and then filled with a fusion gas mixture, e.g., D–T) diffuse into the anode and into the paths of the converging electrons, collision of the electrons with the neutral atoms results in positive ion formation. Farnsworth then argued that if it were assumed that an ion is born or created in that part of the anodic space where the potential difference with respect to the geometric center (shown earlier in Fig. 2.5) is 50 kV, the ion will be accelerated toward the center. An inherent assumption here is that there are few electrons in the vicinity where the ion velocity is low as it reverses direction, avoiding recombination. As previously discussed, the ion will then be trapped between the well potential formed by the potential surface it is born on. Thus, it will oscillate along radial paths through the center. The length of such a path is determined by the potential surface location where the ion was born.

The ions born in the regions adjacent to the anode surface (shown in Fig. 2.5) will accelerate toward the zero potential geometric center with a high acceleration and velocity. All of these ions traversing the geometric center contribute to the high ion density that develops in the "core" region. For the case of 50 kV applied to the grid, the largest contribution to this ion density is attributable to those ions possessing energy in excess of 30 keV, which are presumably ~ 95 % of the total ions in consideration. A rough estimate of the space of heavy ion concentration is that it has a radius around 1 mm. Some of the more slowly moving ions will recombine with an electron near the center and thereby reduce to a neutral atom that tends to drift outwardly. They then will either be reionized with the probability of reappearance of ions of higher energy, or they will escape from the anodic space and be lost. Such reionization of neutral atoms will result in loss of average ion energy or loss from radiation. However, Farnsworth proposed that through intelligent selection of the potential distribution, one could achieve the desired energy ion concentration, $\geq$ 95 %, close to the center.

In short, a sequence of alternating (negative and positive) space charge buildup was proposed by Farnsworth. Such space charges represented either a virtual cathode (negative space charge) or a virtual anode (positive space charge). Farnsworth named this structure as "Poissors" and was illustrated earlier in Fig. 1.3 in Chap. 1.

The Poissor structure formed by monoenergetic radially directed ions and electrons consists of an infinite number of nested well potentials. However, Farnsworth acknowledged that their number would actually be quite limited in practice due to the velocity spread in the ion and electron distributions and also their nonzero angular momentum. This occurs because the points where either the ions or electrons reverse their direction of motion do not lie on mathematically thin surfaces causing the virtual anodes and cathodes or sheaths to have a finite radial thickness. As soon as the distance between a virtual anode and the adjacent virtual cathode approaches this thickness, they will merge and the process of developing alternate virtual electrode ceases.

However, Farnsworth expected the formation of more than one virtual electrode in devices that reduce the velocity spread of ions and electrons. Taking this idea further, he suggested that introducing ions from outside (such as with ion guns) so as to render the ion velocities more uniform, combined with improved electron grid optics to limit

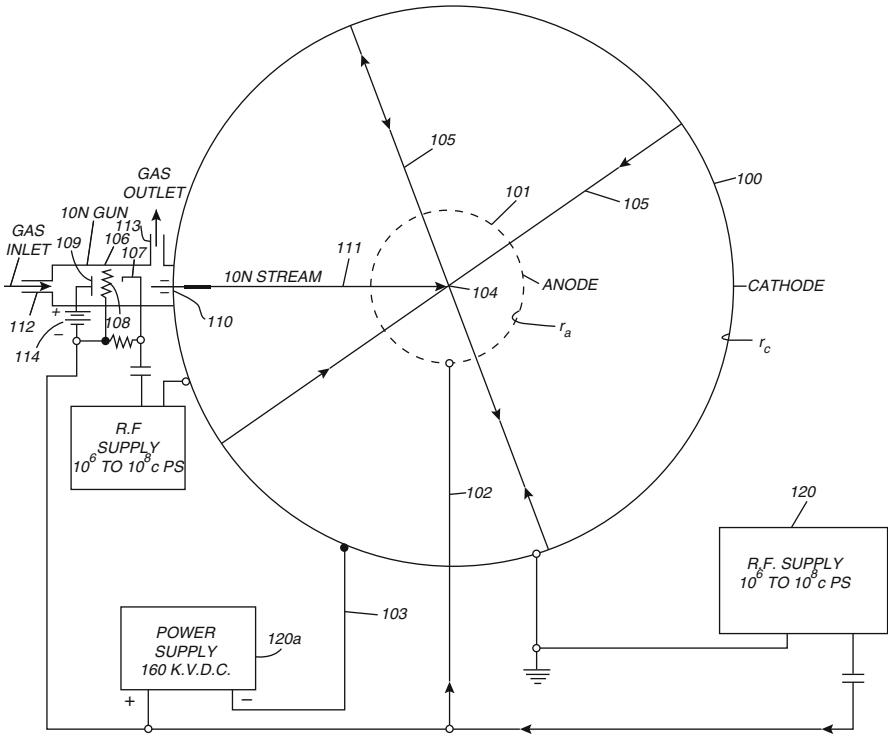

Fig. 2.6 Modification of the IEC design of Fig. 2.5 to add an ion gun, remove the outer grid, and include RF for bunching [6]

their angular momentum, would increase the volume of the ion trap. This idea was picked up on and implemented by Hirsch with his injected ion gun device [6].

2.3.2 *Farnsworth's "Modulation" Concept*

Assuming an ion density of 10^{18} particles/cc in the small volume at the core of the IEC, Farnsworth calculated that if an ion makes 10^6 trips across the core, the probability that the ion will be deflected greater than 8° of arc is only 10 %. He argued that even small deflections greater than the 8° arc would not result in nonradial motion of the ions as they are deflected very near the center, causing the new ion path to be radial as well. Moreover, he suggested the possibility of ion bunching at the core, much like the electrons bunching in a Klystron. To accomplish such bunching, he suggested that the position of the virtual cathode could be shifted radially at a frequency corresponding to the ion oscillatory period. He considered several methods for such a "modulation." One method for shifting the virtual cathode used a radio-frequency voltage between the cathode and anode, as illustrated in Fig. 2.6.

Another method for modulating the cathode is to modulate the ion gun with a radio-frequency voltage from the RF power supply, thus modulating the ion intensity in the ion beam. Assuming that modulation of the anode and cathode is used with a radio-frequency voltage of approximately 150 V in a sine wave profile, the intensity of electron space current converging on the center would also vary periodically, resulting in the oscillatory shifting movement of the virtual cathode as explained previously. As a consequence, the potential gradient accelerating the ions through the center would vary periodically, imparting a corresponding velocity change to the oscillating ions. This will result in some ions traveling faster than others with the consequence that the faster ions will overtake and "bunch" with the slower ions as the center is approached. The ion density in the center is thereby increased. In other words, the ion species that are initially distributed in space are converged a quarter period later at the center (spatially converged) but are then distributed in velocity space at the center.

Such operation provides a very high fusion rate that depends on the square of the density. Depending on the repetition rate, this could lead to a high time average reaction rate. Alternately some applications, e.g., types of neutron activation analysis, favor pulsed neutron production. One of the first studies to incorporate ideas from Farnsworth's bunching concept was done by Edwards [8] at the University of Illinois, and these concepts were extended and incorporated into the Periodically Oscillating Plasma Sphere (POPS) studied by Nebel and Barnes [7]. POPS operation was subsequently experimentally verified. It is truly pioneering on the part of Farnsworth to have intuitively foreseen this kind of behavior of the ions.

Interestingly, Farnsworth made many other pioneering suggestions for optimized operation of the IEC device and some are now being investigated, e.g., the use of vanes instead of wires to build the central cathode [6]. This would help radiate the heat load while reducing the footprint of the cathode wires thus improving the life of the cathode considerably. Another suggestion was the use of boron nitride for constructing the insulating material in the anode stalk; this material has one of the highest standoff voltages and is also easily machineable.

Operation of Farnsworth's IEC concept can be further evaluated by analysis of the ion and electron flow toward the center of the device. The laws by which charged particles move toward the center in a spherically symmetric field have been described by Langmuir and Blodgett as given by Eq. 1.1 in Chap. 1. This equation was originally derived for single species (electrons). However, if ions are present, G_o, defined in Eq. 2.6b, can be introduced. In the following, we change the nomenclature, using λ in the place of G_o, as done in the Farnsworth analysis.

$$\lambda = G_o = \frac{I_i}{I_e}\left(\frac{m_i}{m_e}\right)^{\frac{1}{2}}. \tag{2.46}$$

Farnsworth argued that the space charge formula can be used unchanged, but the denominator of Eq. 1.1 in the new case is now termed as μ^2, which is calculated as a different function of the radius than is α^2. As will become apparent, the term α^2 also

depends upon the factor λ. The quantity λ was introduced by Langmuir [9] wherein it was shown that λ (called α in Langmuir's paper) cannot exceed the value of unity if the ions are injected at the anode. Thus, for the present analysis, Eq. 1.1 is replaced with the following:

$$I_e = \frac{29.34 \times 10^{-6} V^{\frac{3}{2}}}{\mu^2}. \tag{2.47}$$

Here μ is a new function of r/r_c, given in Table 2.1. This table lists the values of ${\mu_a}^2$ and ${\alpha_a}^2$, that is, the values of μ^2 and α^2, respectively, at the anode position as functions of r_a/r_c and with λ as a parameter.

The intermediate values of μ^2 may easily be calculated by dividing Eq. 1.1 by 2.47. This gives (the ratio of electron current in the absence of ions to the electron current in the presence of ions) as follows:

$$\frac{I_{eo}}{I_e} = \frac{\mu^2}{\alpha^2} = \frac{{\mu_a}^2}{{\alpha_a}^2}. \tag{2.48}$$

Here α^2 is obtained mathematically and μ is summarized in Table 2.1.

Consider a small uniform, high-density "core" region at the center of a Poissor-like structure. The ion density in this region is n_o, while its radius is r_o. Taking the maximum cross section of the D–T reaction, the power output of this small region would be given by

$$P_o \approx 10^{-26} {n_o}^2 {r_o}^3 \quad \text{W}. \tag{2.49}$$

Here W corresponds to Eq. 2.4. Further, assuming that the center density is related to an ion current I_o, at r_o by

$$n_o = \frac{I_o}{4\pi {r_o}^2 v_o e}, \tag{2.50}$$

The fusion power output becomes

$$P_o \approx 2 \times 10^{-8} \frac{{I_o}^2}{r_o} \quad \text{W}. \tag{2.51}$$

Here I_o is expressed in amperes. Equation 2.51 emphasizes the fact that the "active" volume in an electrostatic machine would be small, high-density core region rather than a large, moderate-density region, as in most magnetic devices. In a one-meter radius device, a central-region size of $r_o = 0.1$ cm seems reasonable. At that size Eq. 2.51 indicates a total current of 2×10^5 A at $P_o = 10$ kW. This result was encouraging, and Farnsworth decided to undertake corresponding experimental work.

Table 2.1 Various values of α^2 and μ^2 summarized with λ (always < 1) as the parameter

			λ=0.2		λ=0.4		λ=0.6		λ=0.8		λ=1	
$\frac{r_a}{r_c}$ or $\frac{r_c}{r_a}$	α_a^2	$-\alpha_a^2$	μ_a^2	$(-\mu_a)^2$	μ_a^2	$(-\mu_a)^2$	μ_a^2	$(-\mu_a)^2$	μ_a^2	$(-\mu_a)^2$	μ_a^2	$(-\mu_a)^2$
1.6	0.1688	0.2968	0.1330	0.2520	0.0972	0.2071	0.0614	0.1623	0.0255	0.1174	–	0.0730
1.8	0.2480	0.5020	0.2067	0.4431	0.1654	0.3842	0.1240	0.3258	0.0827	0.2664	0.0414	0.2075
2.0	0.3260	0.7500	0.2790	0.6760	0.2321	0.6019	0.1852	0.5278	0.1382	0.5213	0.0913	0.3798
2.2	0.4020	1.0360	0.3497	0.9463	0.2975	0.8566	0.2452	0.7668	0.1930	0.6771	0.1407	0.5874

Note: Here r_a is the anode radius, r_c is the cathode radius, α_a is the value of α when $r = r_a$, μ_a is the equivalent of α_a but in the presence of ions, and μ is the equivalent of α but in the presence of ions

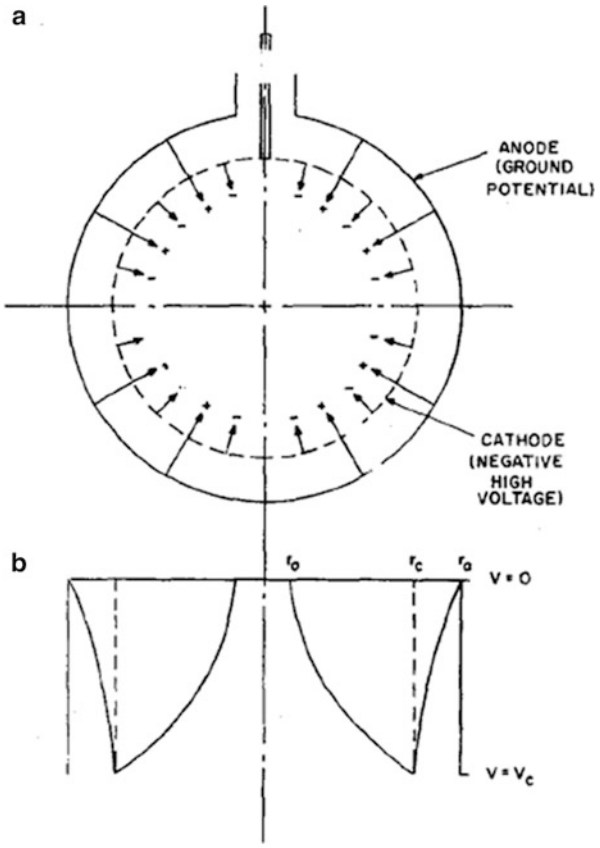

Fig. 2.7 The general arrangement and the potential distributions when ions only are present as assumed by Hirsch [5]

Subsequently, Farnsworth hired Robert Hirsch to work on IEC experiments at the Farnsworth International Telephone and Telegraph laboratory in Fort Wayne, Indiana. Following Farnsworth's work, Hirsch developed a unique six ion gun-based IEC device and published a paper [5, 10] in 1968 reporting the observation of copious number of neutrons. Hirsh considered a spherical cathode and anode (Fig. 2.7a). The cathode is assumed to be ion permeable, electron emissive on its interior surface only, and impermeable to electron flow into the interelectrode space. The anode is assumed to be uniformly ion emissive, and all ions are emitted with zero kinetic energy. Assume that all particle motions are radial, i.e., neglect angular moment and scattering.

For the case of finite ion current and zero electron current, an ion space charge will develop within the cathode. They will form a deep well potential which will be maintained by circulating ions. The associated potential distribution was calculated from a Langmuir–Blodgett-type [11] analysis shown in Fig. 2.7b. The potential at shell, at r_o, represents a virtual anode, i.e., it is a charge-saturated region from which ions are reflected in an outward direction.

For D+ ions at voltages and currents of thermonuclear interest, Hirsch estimates that for a reasonable cathode-to-virtual-anode radius ratio of 10 to 10^2, very high

ion currents of the order of 5 A would be needed. However, he pointed out that with high grid transparency, ion recirculation in the trap between r_c and r_o could exceed 10 round trips, so a more reasonable external current of only 0.5 A would be required. However, if this ion model could be realized experimentally, it would have a negligible fusion rate, since the ion density is low where the ion energy is high near the cathode. The situation changes if electrons are permitted to flow from the cathode. They would be accelerated by the virtual anode toward the center of the device. Once inside the virtual anode, they would be decelerated by their own space charge, and they would form a virtual cathode at $r_{vc} < r_o$. This negative space charge will cause ions from the virtual anode to be accelerated toward the center while also decreasing the radius of the virtual anode. In this manner a series of virtual electrodes would form, creating successively denser regions of high ion kinetic energies.

Hirsch's analysis of this situation [5] starts from Poisson's equation:

$$\left(\frac{1}{r^2}\right)\left(\frac{d}{dr^2}\right)\left[r^2\left(\frac{dV}{dr}\right)\right] = 4\pi(|p_e| - p_i). \tag{2.52}$$

Where the potential at the virtual anode is set to zero, conservation of energy becomes

$$\frac{1}{2}m_i^2 = |eV(r)|, \tag{2.53}$$

$$\frac{1}{2}m_e^2 = e(V - V_0), \tag{2.54}$$

where $V_0 =$ the cathode potential. Conservation of charge becomes

$$I_{e,i} = 4\pi r^2 \rho_{e,i} v_{e,i}. \tag{2.55}$$

Next the radius and the potential are normalized,

$$\phi(r) = \frac{V(r)}{V_0}, \tag{2.56}$$

$$R = \frac{r}{r_a}, \tag{2.57}$$

where $r_a =$ the radius of the virtual anode (note that $\phi(r_a) = 0$). Equation 2.52 then takes the form

$$\frac{d^2\phi}{dR^2} + \frac{2}{R}\frac{d\phi}{dR} = \frac{K_+}{R^2}\left\{\phi^{-\frac{1}{2}} - \lambda_+(1-\phi)^{-\frac{1}{2}}\right\}, \tag{2.58}$$

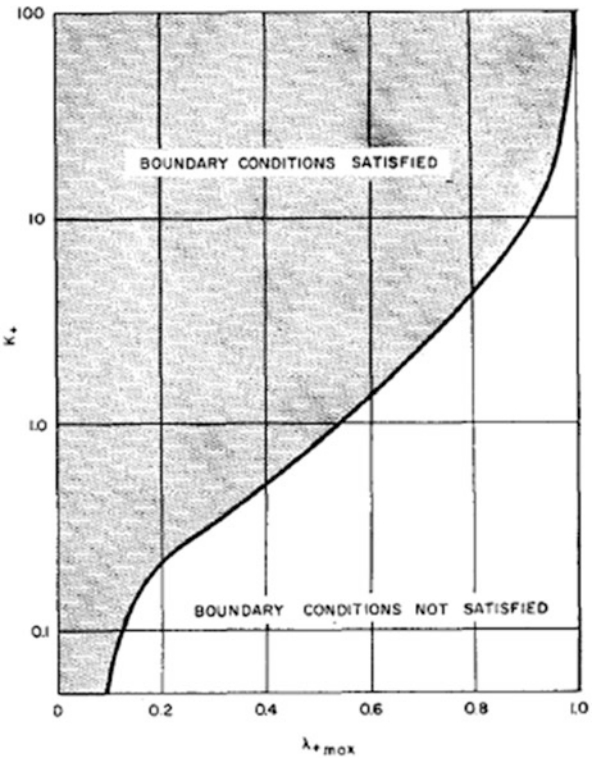

Fig. 2.8 Locus of $\lambda_{+\max}$ as a function of K_+, showing the region in which the boundary conditions are satisfied [5]

where

$$K_+ = \frac{I_i}{|V_0|^{\frac{3}{2}}}\left(\frac{m_i}{2e}\right)^{\frac{1}{2}} = \frac{4\pi r^2 p_i \phi^{\frac{1}{2}}}{|V_0|}, \tag{2.59}$$

$$\lambda_+ = \frac{1}{G_0} = \left(\frac{I_e}{I_i}\right)\left(\frac{m_e}{m_i}\right)^{\frac{1}{2}}. \tag{2.60}$$

Equation 2.60 relates λ_+ used by Hirsch to G_0 defined in Eq. 2.6b. The λ_+ in Poisson's Eq. 2.58 is a key parameter. If $\lambda_+ = 0$, Eq. 2.58 reduces to a form similar to that of Langmuir–Blodgett [10]. To solve Eq. 2.58, Hirsch shows that λ_+ and K_+ must be restricted to meet the boundary conditions. The solution must be carried out in the various regions between the virtual electrodes where the solution is non-determinate due to division by zero (Fig. 2.8).

In the region between the real cathode and the virtual anode, any combination of K_+ and λ_+ to the left of the $\lambda_{+\max}$ curve in Fig. 2.9 will satisfy Eq. 2.58 and the boundary conditions. However, in the region between the first virtual anode and the

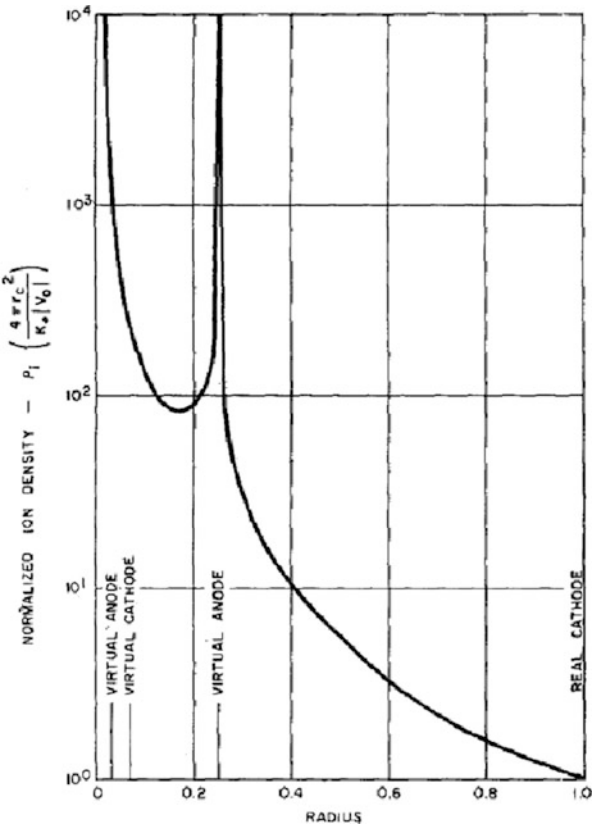

Fig. 2.9 Normalized ion density as a function of radius for $K_+ = 0.7$, $\lambda_+ = \lambda_{+\max} = 0.45$ [10]

inner virtual cathode, both currents are space charge-limited, i.e., they satisfy a K_+, $\lambda_{+\max}$ condition. This condition coupled with the continuity of electron current between the regions is sufficient to determine the ion current in this adjacent region.

A numerical solution using these conditions was shown earlier in Fig. 1.3 in Chap. 1 for $K_+ = 0.7$, $\lambda_+ = \lambda_{+\max} = 0.45$. For convenience this figure is repeated here in Fig. 2.9. Hirsch noted that as expected for this "Poissor" solution, the ion density is more than two orders of magnitude larger at the $R = 0.065$ virtual cathode [10].

Hirsch also addresses the associated issue of pressure balance and the related issue of how the virtual theorem is satisfied. He notes that with purely radial flow, a force balance exists at steady state because the inward and the outward currents of both particles are everywhere equal. In a plane electrostatic system, $E^2/8\pi$ balances the total particle pressure. In spherical geometry such a simple balance does not occur due to the effect of radial focusing [9]. In this simplified analysis the particle pressure is

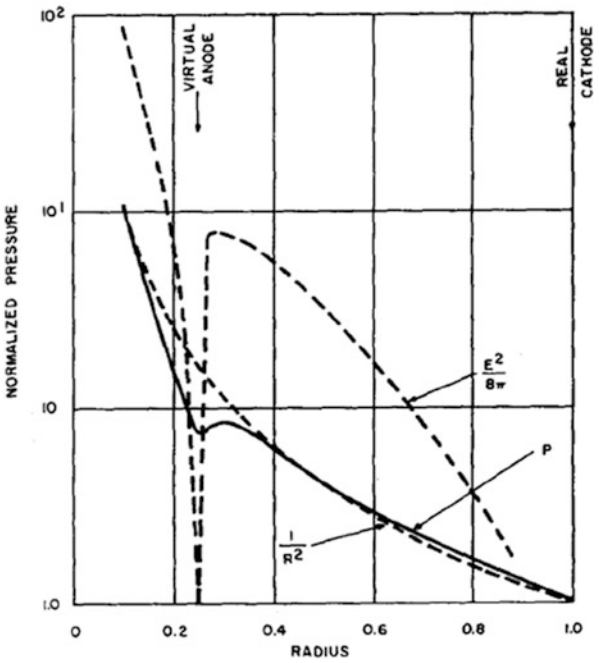

Fig. 2.10 Particle and electric field pressure versus radius for $K_+ = 0.7$, $\lambda_+ = \lambda_{+\max} = 0.45$ [10]

$$P = n_e m_e^2 + n_i m_i^2. \tag{2.61}$$

From Eqs. 2.53, 2.54, 2.55, and 2.59, we obtain

$$P = \left[\frac{(K_+ V_0^2)}{2\pi r_e^2}\right]\left(\frac{1}{R^2}\right)\left\{\lambda_+(1-\phi)^{\frac{1}{2}} + \phi\right\}. \tag{2.62}$$

From again using $K_+ = 0.7$ and $\lambda_{+\max} = 0.45$, Hirsch calculated the particle pressure from Eq. 2.61. It is plotted in Fig. 2.10 along with $E^2/8\pi$. The particle pressure generally follows a $1/R^2$ dependence with the largest deviation occurring at the virtual anode. The electrostatic pressure increases drastically with decreasing radius, but falls to zero at each virtual electrode. In this manner, very high particle and electrostatic pressures are realized near the center of the sphere. It is this dense, high-pressure central region which is of interest to fusion physics. In effect, this analysis shows that this device is not limited by the virial theorem [12]. Two other independent analyses of the generalized electrostatic system have also shown that no such limitation occurs [10]. From a practical point of view, the plasma pressure force in the IEC is ultimately taken up by the grid where the voltage is applied. This is analogous to magnetic confinement fusion where the plasma pressure force must be taken up by the magnetic coil structure.

Hirsch also employs the important features of this model, along with some reasonable assumptions, to determine the general characteristics of an electrostatic fusion reactor. He considers a small uniform, high-density region at the center of a Poissor-like structure. The ion density in this region is n_0, while its radius is r_0. If the reactivity (or power output) is evaluated at a temperature corresponding to the maximum cross section of the D–T reaction, the power output of this small region would be

$$P_0 \cong 10^{-26} n_0^2 r_0^2. \tag{2.63}$$

Assume that the center density is related to an ion current, I_0, at r_0 by

$$n_0 = \frac{I_0}{4\pi r_0^2 v_0 e}. \tag{2.64}$$

Then the fusion power output becomes

$$P_0 \cong 2 \times 10^{-8} \frac{I_0^2}{r_0} \text{W}, \tag{2.65}$$

where I_0 is in amperes. Equation 2.65 emphasizes the fact that the "active" volume in an electrostatic machine would be a small, high-density region rather than a large, moderate-density region, as in most magnetic devices. In a one-meter radius device, a central-region size of $r_0 = 0.1$ cm seems reasonable. At that size, Eq. 2.65 indicates a total ion current of 2×10^5 A at $P_0 = 10$ kW.

2.4 The Polywell: A Spherically Convergent Ion Focus Concept

The electron-injected spherical IEC devices proposed by Elmore, Tuck, and Watson and by Farnsworth in his early patents discussed here have several drawbacks. Grid wires are required to set up the potential trap for electrons, introducing collisional loses and posing materials damage issues in a fusion reactor. Also, as indicated in the analysis by Elmore and colleagues [1], the electron trap may not be adequate to confine the desired ion density needed for an attractive fusion reactor. To circumvent these problems, R. W. Bussard proposed adding a quasi-spherical magnetic field to confine the electrons which in turn electrostatically confines ions [13–15]. His concept was named the Polywell concept (illustrated in Fig. 2.11). Bussard described this as a magnetic version of a spherically convergent ion focus (SCIF) device. In this section we discuss the basic physics involved, largely following the original analysis presented by Krall [16].

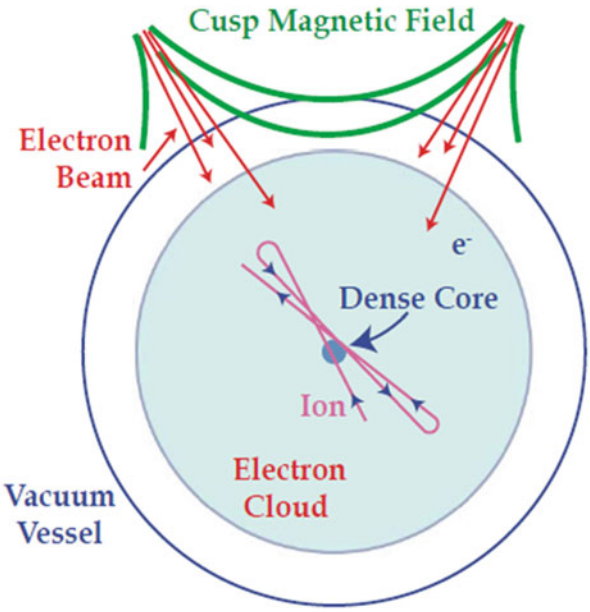

Fig. 2.11 Polywell SCIF schematic [15]

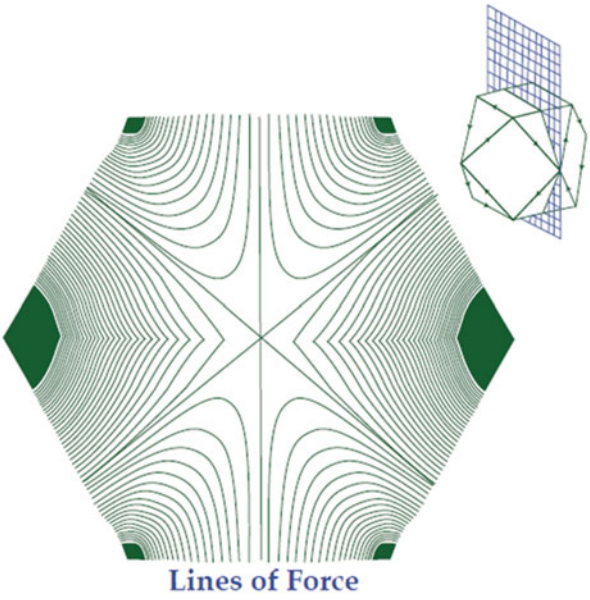

Fig. 2.12 Polywell magnetic geometry showing the magnitude of the *B*-field [15]

The objective is to inject high-energy electrons into a quasi-spherical cusp magnetic field, such as illustrated in Fig. 2.12. Then the electrons, confined by the cusp-like magnetic field, create a well potential of sufficient depth to accelerate ions from low energy at the periphery to fusion energies within a focus at the center of the sphere. Injection of electrons keeps the system electrically non-neutral, so that the well potential, which accelerates the ions, is maintained at a value sufficient to confine the ions within the device, where they circulate at high velocity through the central focus. To succeed, the cusp field needs to confine the electrons long enough so that the power required to maintain the electron "cloud" is less than the fusion power produced by the convergent ion beams. Further, the ions must maintain their radial flow with a nonthermal velocity distribution long enough to produce a high fusion rate in the dense focus at the center of the sphere, as shown in Fig. 2.11.

The power balance in the Polywell device includes the following elements:

1. Energy is largely lost by collisions that scatter the loss cone in the cusp field.
2. Energy is also lost in the magnetic coils that confine the electrons depending on the strength of the magnetic field needed.
3. Energy is produced by fusion in the dense center. The fusion rate there depends on the depth of the well potential (i.e., ion velocity in the center core) plus the degree of spherical focus in the ion flow (i.e., ion density in the center core).

The magnetic geometry is magnetohydrodynamically (MHD) stable by the nature of using cusp fields. Still, as in all IECs, the plasma in this device must be far from thermal equilibrium, and the ion velocity distribution should be far from Maxwellian. For magnetic confinement of electrons, their orbits in the magnetic field must be small compared with the size of the device. By contrast, the ion orbits can be comparable to the size of the device, consistent with the idea that electrostatic effects dominate the ion orbits. However, the orbits of the MeV fusion products (e.g., the 3.5-MeV alpha particle from D–T fusion, the 14.7-MeV proton from D–^{3}He, or the ~ 4-MeV alpha particles from p–B^{11}) will be much larger than the size of the device because they are much more energetic than the fuel ions. Thus, direct conversion of energy to electricity of these fusion products becomes an appealing possibility. Any neutrons created will, however, escape, and their energy must be recovered as heat in a "blanket" region such as envisioned for magnetic confinement fusion.

The basic magnetic geometry that confines electrons in the Polywell device is illustrated in Fig. 2.12. The magnetic field lines are shown on a plane through the center of the device. In the third dimension, the magnetic field continues to be a set of point cusps arranged in an alternating pattern in a generally spherical geometry. This quasi-spherical field arrangement is the basis of the Polywell concept but can correspond to various orders of polyhedra. The lines shown correspond to an $m = 3$ configuration, called a truncated cube, with $B = B_o(r/R)^m$ fairly near the center of the configuration, where R is the radius of the device.

Electrons are injected into this geometry from electron guns at high energy because the maximum depth of the well potential created will be approximately equal to the incoming electron energy. The current from the gun must be chosen to

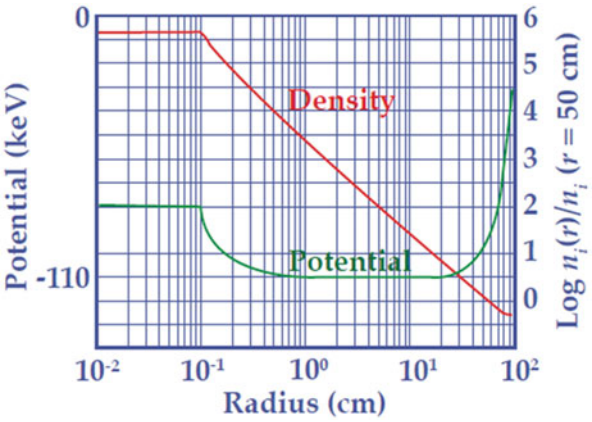

Fig. 2.13 Typical well potential profile [15]

balance the electron losses, which are twofold. First, losses directly through the cusps are inversely proportional to the strength of the magnetic field. The "standard" expression for the single point cusp confinement time t_c is [15]:

$$t_c = t_{transit} \frac{R^2}{a_0^2}, \tag{2.66}$$

where a_0 is the electron gyroradius and the gyration time is $t_{transit}$. The second loss mechanism comes from transport across the magnetic field, either due to collisions or to fluctuating electric and magnetic fields created by plasma instabilities. Estimates are that the cross field losses are relatively low, but more study is required to confirm this.

Another energy loss q_{br} associated with electrons is radiation, including synchrotron and Bremsstrahlung radiation, which is given by [14]:

$$q_{br} = 7 \times 10^{-38} {n_e}^2 T_e r_e \ \mathrm{W/m^3}, \tag{2.67}$$

where r_e is the radius (meters) over which the electrons have density n_e in electrons/m^3 and temperature T_e in eV. This loss is predominantly from the dense core region due to the ${n_e}^2$ dependence.

The effect of radiation losses on the power balance is complicated because the electron temperature must be determined consistently with the other physics of the system. As already stated, for successful operation, $T_e \ll T_i$.

In the Polywell, the ions are electrostatically confined in the device as a whole but are not confined in the dense center of the device. A potential of the sort shown in Fig. 2.13 will be produced because of the excess of electrons in the plasma, enforced by injection of energetic electrons from the guns. As shown, the well potential is formed, in this case with a depth of -110 keV. The ion density is shown

peaking in the center of the device due to the spherical convergence of the accelerated ions. The increased ion density in this "core" region causes the well potential to decrease in depth there to about −80 keV. The ion orbits will consist of large-scale radial excursions from + R to −R passing through the center of the well potential on each pass. Thus, the ions in the center of the device are transitory and highly non-Maxwellian. In summary, according to the calculations shown in Fig. 2.13, the ion orbits are indeed large scale, i.e., they do not gyrate in the cusp magnetic field but instead oscillate from boundary to boundary. Further, this oscillation produces a high-density region in the center of the device.

Next we consider the ion orbits. Assume that an ion is born with a low energy E_0 of a few electron volts at a location r_o and with comparable radial and azimuthal velocities v_r and v_i. Now assume that the ion enters an electrostatic potential $\phi(r)$ and magnetic field $B = B_o(r/R)^m$. To estimate whether the ion will reach $r = 0$ or instead be reflected by the magnetic field, for simplicity we consider a one-dimensional slab-like model [(x, z) coordinates].

$$v_0 = v_{x0}\hat{x}\,, \phi = \phi(x), B = B_0(x/R)^m\hat{z}\,. \tag{2.68}$$

Then the ion orbits can be written in terms of their $\hat{x}$ velocity. Krall [16] shows that integration from the ion birth point x_o to an interior point x gives (setting $v_{yo} = 0$)

$$v_x^2 = v_{x0}^2 - 2e\left[\frac{\phi(x) - \phi(x_0)}{m_i}\right] - \frac{\omega_{ci}^2}{(m+1)^2 R^{2m}}\left(x^{m+1} - x_0^{m+1}\right)^2. \tag{2.69}$$

Here ϕ_0 is presumed to decrease as x decreases, and $\omega_{ci} \equiv eB_o/m_i$. Also, $m = 0$, 1, 2, ... defines the curvature [16]. By examination of Eq. 2.69, the ions will reach $x = 0$ without reflection if

$$\frac{eB_0}{m_i}\left(\frac{x_0}{R}\right)^m \frac{x_0}{m+1} < \sqrt{\frac{2e\phi_0}{m_i}}, \tag{2.70a}$$

where ϕ_0 is the maximum depth of the well potential produced by the electron cloud. This means that the maximum birth velocity and local cyclotron frequency must satisfy

$$\frac{v_{\max}}{\omega_{c,\max}} > \left(\frac{x_0}{R}\right)^{m+1} \frac{R}{m+1}, \tag{2.70b}$$

if the ions are to have orbits as large as x_0.

This result (Fig. 2.14) shows that an ion born in a strong electrostatic potential will transit the entire geometry of size R, even when the gyroradius calculated from the velocity and magnetic field at the ion birth point is much smaller than R. We can

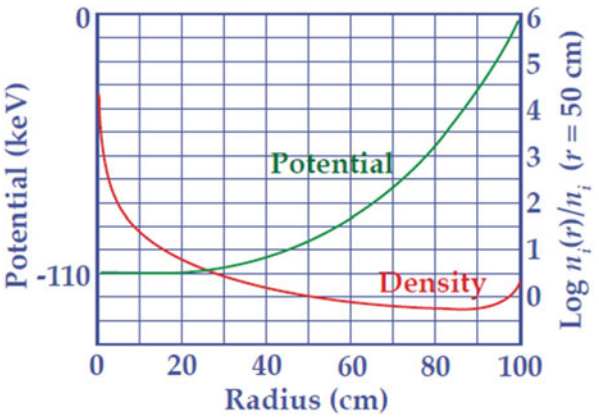

Fig. 2.14 Typical ion density profile [15]

also estimate the perpendicular deflection of the ion by the magnetic field during its transit through the core region of the well potential as

$$\frac{\Delta V}{V} = \frac{\omega_{ci}^2}{(m+1)^2}\left(\frac{x_0}{R}\right)^{2m}\frac{x_0^2}{\left(\frac{2e\phi_0}{m_i}\right)}, \tag{2.71a}$$

where

$$\Delta v_y \simeq \sqrt{v_x^2 - v_{x0}^2 + \frac{2e[\phi(x) - \phi(x_0)]}{m_i}}. \tag{2.71b}$$

This result shows that the maximum magnetic field allowed at the ion birth point in order for the ion to converge to a spot δr is

$$\delta r = R\left(\frac{\Delta V}{V}\right). \tag{2.72}$$

We next estimate the ion density in the Polywell due to spherical convergence. Assume that at birth the ion distribution function is uniform in energy up to some small energy E_0, and uniform in angular momentum up to some small azimuthal velocity $v_\perp$, and take the potential at the birth point to be $\phi = 0$. This distribution can be described in terms of the constants of the motion $\left[E = \left(\frac{1}{2}\right)m_i\left(v_r^2 + v_\perp^2\right) - e\phi, rv_\perp\right]$ by the function:

$$F = \begin{cases} 3\left(\frac{m_i}{E}\right)^{\frac{3}{2}} n_{edge}, 0 < E < E_0, 0 < rv_\perp < r_0 v_{\perp 0} \\ 0, \ otherwise \end{cases}. \tag{2.73}$$

The Vlasov equation for steady state is $F(E, rv_\perp) =$ constant, so the density everywhere is determined by the potential and the value of F at the ion birth point. Integrating F over velocity determines the density. There are three distinct density regions. For a very small distance from the birth point, the potential is negligible, and the density is given by $n = n_{edge}$. Because the maximum well depth is in the keV range, compared with ion birth energies in the few eV range, a little way toward the center $E_0 \ll 2e\phi$ and $m_i {v_{\perp 0}}^2 (R/r)^2 < 2e\phi$. In that range, the electron density n_e is given by integrating Eq. 2.73 over $v_\perp dv_\perp dv_r$ with the result:

$$n_e = \frac{3}{4}\sqrt{\frac{E_0}{e\phi}}\left(\frac{R^2}{r^2}\right)n_{edge}. \tag{2.74}$$

Assuming that the potential reaches its full value at a moderately large distance from $r = 0$, we see that the electron density throughout the bulk of the device will be of the order (set $r = R/2$ in Eq. 2.74):

$$n_e = n_0 = 3n_{edge}\sqrt{\frac{E_0}{e\phi_{\max}}}. \tag{2.75}$$

Moving inward, the $(R/r)^2$ factor eventually becomes substantial, so that the density becomes much larger than n_0. Eventually, the radius is so small that $M{v_{\perp 0}}^2 (R/r)^2 > 2e\phi_{\max}$. Inside that radius, the density changes fairly slowly, on the scale of the changing potential. This defines the radius of the dense core r_c as the radius at which $2e\phi = m_i {v_{\perp 0}}^2 (R/r)^2$ because $n \sim 1/r^2$ outside that radius, while inside that radius n is nearly constant, with the value

$$n_e = \sqrt{\frac{m_e v_{\perp 0}^2}{2e\phi_{\max}}}R. \tag{2.76}$$

Thus, the ion orbits are seen to be of the size of the device, and the ion density at the center is large, $n_i \sim (R^2/{r_c}^2)n_0$. The size of the core and the central density are seen to depend on the angular momentum at the outer turning points of the ion motion. A typical ion density profile based on these assumptions was shown in Fig. 2.13.

If the performance follows these estimates, the Polywell configuration offers a number of advantages as a fusion reactor. It offers a high-beta geometry with no complex auxiliary heating or confinement systems; in practice, this means that the scheme can be tested with a fairly modest budget and with a fairly short development path. The trade-off, of course, is that the physics of the device is not simple at all, encompassing a highly nonequilibrium system with widely varying parameters at different radial points in the device.

It is clear from the assumption made in this analysis that there are a number of critical physics issues. One of the most important pertains to electron physics.

Electron losses will be a major energy drain on the system. Favorable energy balance will depend on the electron confinement time not being too much shorter than classical. Yet cusp losses are not a particularly well-established concept. If the single particle lifetime in a cusp field is calculated, the confinement time will resemble mirror confinement, with the effective collision time being comparable with a particle transit time. This is because in a single pass the particles lose track of their magnetic moment when they pass through the low-field region. Numerical calculations of single particle orbits in a cusp confirm this picture. Mirror losses with transit time collisions are not acceptable. However, when a plasma fills the cusp, magnetic field is excluded, and the $\beta = 1$ surface becomes a mod-β = constant surface. The transport picture is then expected to revert to the cusp picture, with a much longer confinement time. The ability to establish this high-beta plasma, which Krall [16] termed the "wiffle ball" mode, in order to reduce electron loss is a central issue for the Polywell scheme. The "wiffle ball" mode greatly reduces electron losses through the cusp loss cones if it can be achieved. One potential problem for experiments is that very high electron injection rates may be required to reach the high β "wiffle ball" mode. This is due to the fast loss rates through the cusps that occur before the favorable "wiffle ball" confinement mode is achieved. Once that occurs, the injection rate can be reduced, but this injection rate "barrier" must be met and sets the rating needed for electron gun injection.

2.5 Summary

This chapter has focused on well potential formation and fully ionized spherical IECs. Other geometries have also been studied to see whether such wells could be formed. One example is a gridded cylindrical device that can be viewed as a two-dimensional version of the spherical IEC. However, a spherical geometry has generally been favored due to the three-dimensional convergence of the ion beam in the central core. Such convergence has been viewed as important due to the reaction rate dependence on the density square. In order to eliminate the background neutral pressure, the ions must be generated externally and "injected" into the device. As stressed, this presents a problem because the desire is to have the ions born at an energy slightly below that of the outside anode or chamber wall.

The picture is similar but the voltages are reversed in an electron-injected type IEC. An analytical solution to space charge effects and well potential formation is difficult and requires a number of simplifying assumptions. Typically these include no background neutrals; monoenergetic/no angular momentum; nearly 100 % transparent grid; and symmetry of potential surfaces, including the high-voltage stalk area.

We have reviewed the early study by Elmore, Tuck, and Watson which assumed electron injection. For illustration we obtained a first order solution ($G_0 = 0$) given by Eq. 2.10. This result, however, restricts the fusion core volume such that high fusion powers do not appear feasible. It might be noted, however, that such a device

would be small and relatively inexpensive but still demonstrate fusion breakeven. When the restriction $G_0 = 0$ is relaxed, larger core volumes are possible but thermalization effects are found to require extremely large ion currents of the order of 10^{14} A. Even though this is a simplified solution, it errs on the optimistic side. In view of these disappointing results, various modifications to the basic IEC device have been proposed by other researchers. For example, the Polywell concept proposed by R. W. Bussard (described in Chap. 1) employs a magnetic field to confine the electrons, thus simplifying the problem of obtaining a larger trap region and, hence, fusion volume. While Philo Farnsworth initially studied several modified electron-injected devices, he and Robert Hirsch ended up studying an ion-injected IEC both theoretically and experimentally. The theory for this led to the multiple potential trap profile shown in Fig. 1.4, where the ion density and, hence, fusion rate increase in each potential trap going toward the center line of the device. It is difficult to take advantage of this effect, however, because as already stated only a single potential trap seems possible in practice. In that case, the reaction volume is again small, presenting a problem. The volume can be increased by adding angular momentum to the injected ions, but in doing that the required ion currents become progressively larger. These issues related to the practicality of fusion power devices are discussed further in a later chapter.

References

1. Elmore WC, Tuck JL, Watson KM (1959) On the inertial electrostatic confinement of a plasma. Phys Fluids 2(5):239
2. Yibin G, Miley GH (2000) Experimental study of potential structure in a spherical IEC fusion device. IEEE Trans Plasma Sci 28(1):331–346
3. Tzonev IV, Miley GH, Nebel RA (1995) A computational study of the convergence of large angular momentum, high current ion beams in an inertial electrostatic confinement (IEC) device. In: International conference phenomena in ionized gases XXII, vol 4, pp 197–198
4. Farnsworth PT (1966) Electric discharge device for producing interaction between nuclei. US Patent 3,258,402
5. Hirsch RL (1967) Inertial electrostatic confinement of ionized fusion gases. J Appl Phys 38(11):4522–4534
6. Farnsworth PT (1966) US Patent 3,258,402
7. Edwards BE (1979) Ion dynamics in a spherical reflex diode. Ph.D. thesis, University of Illinois at Urbana–Champaign
8. Nebel RA, Barnes DC (1998) The periodically oscillating plasma sphere. Fusion Technol 34(1):28–45
9. Langmuir I (1929) The interaction of electron and positive ion space charges in cathode sheaths. Phys Rev 33(6):954
10. Hirsch RL (1968) Experimental studies of a deep, negative, electrostatic well potential in spherical geometry. Phys Fluids 11(11):2486
11. Langmuir I (1913) Phys Rev 2:450; Physik Z (1914) 15:348; Langmuir I, Blodgett KB (1923) Phys Rev 22:347; 23, 49 (1924)
12. Clausius RJE (1870) On a mechanical theorem applicable to heat. Philos Mag Ser 4(40):122–127

13. Bussard RW Method and apparatus for controlling charged particles. US Patent 4,826,626, 2 May 1989
14. Bussard RW et al. (1988) Preliminary research studies of a new method for control of charged particle interactions. Report 1899, Pacific Sierra Research, 30 Nov 1988
15. Bussard RW (1991) Some physics considerations of magnetic inertia electrostatic confinement: a new concept for spherical converging flow fusion. Fusion Technol 19:273
16. Krall N (1992) The Polywell: a spherically convergent ion focus concept. Fusion Technol 22:42–49

http://www.springer.com/978-1-4614-9337-2

Inertial Electrostatic Confinement (IEC) Fusion
Fundamentals and Applications
Miley, G.H.; Murali, S.K.
2014, XVIII, 400 p. 292 illus., 200 illus. in color.,
Hardcover
ISBN: 978-1-4614-9337-2